

The role of Ag–O–Al species in silver–alumina catalysts for the selective catalytic reduction of NO_x with methane

X. She, M. Flytzani-Stephanopoulos*

Department of Chemical and Biological Engineering, Tufts University, Medford, MA, USA

Received 5 July 2005; revised 21 September 2005; accepted 26 September 2005

Available online 23 November 2005

Abstract

We examined the role of silver and alumina in Ag–alumina catalysts for the selective catalytic reduction (SCR) of NO_x by methane in gas streams containing excess oxygen. A cogelation technique was used to prepare Ag–alumina materials with high dispersion of silver even at high metal loadings (>10 wt%) and after air calcination at 650 °C. Typically, a part of silver is present as fine nanoparticles on the alumina, whereas another part is ionic, bound with the alumina as [Ag–O–Al] species. Dilute nitric acid leaching was used to remove the silver particles and all weakly bound silver from the surface of these materials. Complementary structural characterization was performed by HRTEM, XPS, XRD, and UV–vis DRS. We found that the higher the initial silver content, the higher the amount of the residual [Ag–O–Al] species after leaching. NO–O₂–TPD tests identified that silver does not modify the surface properties of the alumina. The SCR reaction-relevant NO_x adsorption takes place on alumina. Temperature-programmed surface reaction (TPSR) and kinetic measurements at steady state were used to check the reactivity of the adsorbed NO_x species with methane and oxygen to form dinitrogen. Only the alumina-adsorbed nitrates react with CH₄ to produce N₂ in the presence of oxygen, beginning at ~300 °C as found by TPSR. Moreover, the SCR reaction rates and apparent activation energies are the same for the leached and parent Ag–alumina catalysts. Thus, metallic silver nanoparticles are spectator species in CH₄-SCR of NO_x. These catalyze the direct oxidation of methane at temperatures as low as 300 °C, which explains the lower methane selectivity for the SCR reaction measured over the parent samples.

© 2005 Elsevier Inc. All rights reserved.

Keywords: Silver; Alumina; Leaching; Silver aluminate; Selective catalytic reduction of NO; Methane oxidation; Selectivity; Nitrogen oxides; TPD; Temperature-programmed surface reaction

1. Introduction

The selective catalytic reduction (SCR) of NO to N₂ with hydrocarbons is a promising technology for NO_x removal, having attracted much attention for nearly two decades. Initial studies were focused on zeolites loaded with metals, such as Cu, Co, Ga, In, and Pd [1–12], since zeolites are well known to stabilize metal ions, the presence of which is deemed necessary for the SCR reaction. However, zeolite-based catalysts suffer from deactivation in water vapor- and sulfur dioxide-containing exhaust gas streams, which renders them less attractive for practical applications. Metal oxide catalysts have been examined as alternatives due to their high hydrothermal stability. A recent

review by Burch et al. [13] discusses these types of catalysts, which include rare earth oxides (REO) and alumina- (or other oxides) supported Pt, Ga, In and Pd catalysts. The platinum group catalysts are active at low temperatures, but are limited by a narrow operating temperature window in which they display good selectivity. They are also more selective to undesired N₂O, a potent greenhouse by-product. Ga and In catalysts are limited by loss of activity in the presence of water; and Pd catalysts are inhibited by excess of oxygen in the exhaust gas stream. Other reports in the literature point to the enhancement of both activity and stability using sulfated alumina or zirconia as supports for Pd [14–16], Mn [17] and Co [18,19] for the SCR of NO with methane. The acidity of these supports was considered key to stabilizing the active state of the metal species.

Since Miyadera et al. [20] reported that silver/alumina catalysts exhibited relatively good activity and selectivity for NO

* Corresponding author.

E-mail address: mflytzan@tufts.edu (M. Flytzani-Stephanopoulos).

reduction to N_2 and moderate resistance to water and sulfur dioxide, many studies have been performed on this catalyst system [21–41]. The most commonly used reductants are propane/propene [20–27], but there have also been reports on using higher hydrocarbons [28–33]; oxygenated hydrocarbons [34–40]; and even methane [41] as reducing agents. Higher hydrocarbons were found to shift the active temperature window to lower values and increase the tolerance to water [28]. In particular, using octane as the reductant has attracted much interest in the recent literature [30–33], with reported light-off temperature as low as 250 °C and optimal C:N ratios of 4–6. Interestingly, it has been reported that gas-phase reactions past the catalyst bed can contribute to the reduction of nitric oxide to dinitrogen [30,31]. However, a significant drawback of using octane as a reductant is the significant formation of CO accompanying the NO reduction reaction. With oxygenated hydrocarbons, high NO conversions can be obtained at 250–400 °C; however, the main problem is the formation of a large amount of harmful nitrogen-containing byproducts [34–40]. An important finding for the Ag/alumina system is that the activity for NO reduction is strongly correlated to the silver loading, and the most active Ag–alumina catalysts have been reported to contain 1.2–3 wt% Ag [23–26,31,33,41]. Structural analysis identified oxidized silver in the SCR-active Ag/alumina catalysts of intermediate silver loading, whereas metallic silver particles or Ag_n^0 clusters were dominant in the high-silver content alumina catalysts, which were less selective for NO reduction and were good for the direct combustion of hydrocarbons [23–26,29,41]. This also holds true for methane. In their study of methane combustion over Ag/ZrO₂, Kundakovic et al. [42] found that metallic Ag nanoparticles (oxygen-covered) are excellent catalysts for the direct oxidation of methane.

In addition to the change in the silver oxidation states, Wang et al. [43] explained the loading effect of silver on alumina as relating to acidity changes of the alumina surface. Finally, another type of structure, silver–aluminate, has been suggested as important for NO SCR [22,23]. Nakatsuji et al. [44] obtained a $AgAlO_2/Al_2O_3$ catalyst by hydrothermal treatment at high temperature that was even more active than the respective Ag/Al₂O₃ catalyst. However, it has also been observed that silver phases exhibit significant mobility under SCR reaction conditions [26,27], thus contradicting the proposal of stable silver aluminate.

The proper synthesis method is crucial to the preparation of catalysts with desirable silver structures. Impregnation methods are limited by silver particle aggregation at relatively high silver loadings [23–26], and the catalysts thus prepared have a very narrow active temperature window. In contrast, coprecipitation-gelation methods have been found to better disperse and stabilize oxidized silver, possibly due to better interaction of silver species with the alumina during the gelation process [41,45,46]. A broader active temperature window was reported for a 5 wt% Ag–Al₂O₃ prepared by a sol–gel technique [46]. In our previous work, Ag–alumina catalysts prepared by a single step co-gelation method [41] were active for the SCR of NO with methane in excess O₂. Silver ions and silver oxide clusters were

found to dominate in the SCR-active (3.2 wt% Ag) catalysts by UV–vis DRS [41].

Thus, evidence points to oxidized silver on alumina as the NO-SCR sites and attributes the loss of selectivity to the presence of silver nanoparticles, which catalyze the direct oxidation of the hydrocarbon, including methane [23,41,42]. However, this general picture cannot explain how methane is activated on silver aluminate structures. Is the presence of silver particles needed for this? How does the presence of silver modify the alumina surface? In a recent paper [47], the importance of Ag^+ ions for CH₄-SCR of NO was shown using Ag-ZSM-5. Activation of CH₄ was suggested to occur on isolated Ag ions in the zeolite. It is of interest to investigate the role of silver ions for CH₄-SCR of NO in Ag–alumina catalysts with no silver particles present. To our knowledge, no such particle-free Ag–alumina catalysts have been examined in the literature. Even with the most active, low-content silver–aluminas, some silver particles were always present, depending on the preparation method and calcination temperature.

In this work, dilute nitric acid leaching was used to successfully remove metallic silver particles from the as-prepared Ag–alumina catalysts. The resulting Ag–O–Al surfaces were characterized and compared with unmodified aluminas, and in kinetic experiments the role of silver particles for the CH₄-SCR of NO was clarified by comparing the leached and parent catalysts.

2. Experimental

2.1. Catalyst preparation

2.1.1. One-pot co-gelation method

Ag–alumina catalysts were prepared by a one-pot coprecipitation-gelation method as described previously [41]. Accordingly, aluminum nitrate (Fluka, 99% or Alfa, 98%) and silver nitrate (Aldrich, 99.995%) were used as precursors. After the desired amount of these two nitrate salts was dissolved in deionized water, the precipitation agent, tetramethylammonium hydroxide solution (25%, Fluka), was added dropwise at room temperature until a yellow/gray-colored precipitant appeared (pH = 10–11). This was left to gel at this condition for 12 h, then filtered, washed with deionized water several times, and dried in a vacuum oven (25 in Hg, 60 °C) for 10–12 h. The dried solid was crushed thoroughly, then heated at a rate of 2 °C/min up to 650 °C and kept at this temperature for 5 h. The elemental compositions of the final catalysts were analyzed by inductively coupled plasma (ICP) using a Leeman Labs PS-1000 instrument. The as-prepared Ag–alumina catalysts are denoted as AlAg(*x*,CG), where *x* is the wt% of Ag and CG denotes the coprecipitation-gelation method applied.

2.1.2. Nitric acid leaching

Leaching by dilute nitric acid solutions was the technique chosen to remove weakly bound silver from the Ag–Al₂O₃ samples by immersing each sample (~1.5 g) in 100 ml of 10% HNO₃ at room temperature for 8 h. After leaching, the recovered solids were washed with deionized water several times,

dried in a vacuum oven (25 in Hg, 60 °C) for 10–12 h, and heated at a rate of 2 °C/min to 650 °C and kept there for 3 h. Again, ICP analysis measured the amount of residual silver in the leached catalysts. The leached samples are denoted as AlAg(*x*, L), where *x* is the wt% of Ag, and L indicates a leached sample.

2.2. Catalyst characterization

The BET specific surface area of each sample was measured by single-point N₂ adsorption/desorption on a Micromeritics Pulse Chemisorb 2705 instrument. HRTEM/EDS was performed on a JEOL 2010 instrument equipped with a LaBr₆ electron gun source with a resolution of 0.14 nm. The microscope was operated at 200 kV, and had an attachment for X-ray dispersive spectroscopy (EDS) for elemental analysis of selected areas. The catalyst preparation involved suspending the sample in isopropyl alcohol in an ultrasonic bath and then depositing it on a carbon-coated 200-mesh Cu grid.

X-Ray powder diffraction (XRD) analysis was performed on a Rigaku 300 X-ray diffractometer. Copper-K_α radiation was used. The tube voltage was 60 kV, and the current was 300 mA.

The oxidation states of silver and the atomic ratio of silver to aluminum in the surface region of the Ag–alumina catalysts were examined on a Perkin–Elmer Model 5200C X-ray photoelectron spectrometer (XPS), with an Al-K_α anode used as the X-ray source. All samples tested by XPS were in as-prepared form. Each powder sample was pressed onto a copper foil, then placed into the vacuum chamber without any pretreatment. The Al 2p signal of Al₂O₃ was used as internal reference to correct the XP spectra [25]. The atomic ratio of Ag/Al was based on the core level spectra of Ag 3d and Al 2p.

UV–vis diffuse reflectance spectra (DRS) were collected with a Hewlett Packard 8052A diode array spectrophotometer equipped with a diffuse reflectance attachment (DRA) (Harrick). The UV–vis spectra of alumina and Ag–alumina samples were collected at room temperature in air in the range of 190–820 nm with a resolution of 2 nm. MgO powder (99.99%, Aldrich) was used as a reference.

2.3. Microreactor activity tests

Catalyst activity tests were performed in a quartz tube (1 cm i.d.) packed-bed flow microreactor. The catalyst powder (finely ground) was held with a layer of quartz wool on a quartz frit at the center of the reactor. The reactor was heated inside an 800-W Lindberg furnace. A K-type thermocouple embedded in the catalyst bed from the top of the reactor and connected to an Omega temperature controller was used to monitor the bed temperature. Four gas mixtures of grade 5 purity (3% NO/He, 10% CH₄/He, 20% O₂/He, and pure He) were blended to achieve the desired reaction gas stream composition. Each feed gas flow rate was measured and controlled independently by a mass flow controller. All tests were performed at atmospheric pressure.

Most tests were conducted under a reactant gas composition of 0.25% NO–2% CH₄–5% O₂/He and a space velocity of 9000 h⁻¹ (NTP). Typically, a 0.4 g sample load and a gas flow

rate of 100 ml/min were used at this space velocity. The samples were tested in the temperature range of 300–700 °C in 50°-steps. At each temperature, data were collected for 1–1.5 h after steady state was established. After the ascending-temperature tests, descending-temperature tests were run to check for possible catalyst deactivation. The product gas stream was analyzed by a gas chromatograph (HP 5890) equipped with a 10-ft × 1/8-inch diameter 5A molecular sieve column and a thermal conductivity detector (TCD). NO, CH₄, O₂, N₂, and CO species could be separated by this column. Catalysts were ranked by comparing the values of *x*_{NO}, *x*_{CH₄}, and *S*_{CH₄}, representing conversion of NO to N₂, conversion of CH₄ to CO_{*x*}, and selectivity of CH₄ for NO reduction, respectively, defined as follows:

$$x_{\text{NO}} = \frac{2[\text{amount of N}_2 \text{ produced}]}{[\text{initial amount of NO}]}, \quad (1)$$

$$x_{\text{CH}_4} = \frac{[\text{amount of reacted CH}_4]}{[\text{initial amount of CH}_4]}, \quad (2)$$

$$S_{\text{CH}_4} = \frac{2[\text{amount of N}_2 \text{ produced}]}{[\text{amount of reacted CH}_4]}. \quad (3)$$

2.4. Reaction rate measurements

Reaction rate measurements were made using the same reactor system as described above. Samples with a particle size of 53–150 μm were used for these tests. To keep the reactions in the kinetic regime, the conversion of NO was kept at <10% and the conversion of CH₄ was <30%. Typically, the reaction rates were measured in a feed gas mixture of 0.5% NO–0.5% CH₄–5% O₂/He at a temperature range of 425–525 °C. Steady-state rates were recorded at each temperature. After measurements in the ascending mode, temperatures were reduced and measurements repeated in the descending mode, which also checks for any catalyst deactivation. A blank test was also performed with empty reactor at the above conditions to check for gas-phase reactions.

The rate of NO reduction to N₂ ($-r_{\text{NO}}$) and the overall CH₄ oxidation rate ($-r_{\text{CH}_4}$) were calculated as follows:

$$-r_{\text{NO}} = F_{\text{NO}} X_{\text{NO}} / W \text{ (mol/(g s))} \quad (4)$$

and

$$-r_{\text{CH}_4} = F_{\text{CH}_4} X_{\text{CH}_4} / W \text{ (mol/(g s))}, \quad (5)$$

where *W* is the catalyst loading (in g), *F_i* is the molar flow rate (*i* = NO, CH₄, in mol/s), and *X_i* is the conversion of NO to N₂ or CH₄ to CO_{*x*} (*i* = NO, CH₄). Reaction rates, normalized by the surface area, were calculated by dividing these rates by the initial specific surface area of each sample. Apparent activation energies were calculated from Arrhenius-type plots of the reaction rate.

2.5. Temperature-programmed desorption (TPD) tests

NO–O₂-TPD was performed to study the surface adsorption of NO on the various types of catalysts in the presence of O₂, as is the case under SCR conditions. NO and O₂ were used as adsorbates. TPD tests were performed in a quartz fixed-bed

flow reactor (1 cm i.d.) coupled to a quadrupole mass spectrometer (MKS-PPT-200EM). Generally, 0.1 g of catalyst was held between two layers of quartz wool in the reactor. The temperature was controlled by a thermocouple in contact with the upper layer of quartz wool. The sample was pretreated at 500 °C for 1.5 h in 50 ml/min of pure helium, then cooled to room temperature in helium. A gas stream of 1.5% NO–5% O₂ at 50 ml/min was then flowed over the sample until the NO and O₂ signals monitored by the mass spectrometer leveled off, normally around 2.5 h. Then the catalyst was purged with helium for ~10 h to remove any weakly adsorbed species. Desorption was performed by flowing 50 ml/min He or 5% O₂/He (to simulate the lean-burn condition with excess O₂) and ramping the temperature from ambient temperature to 700 °C at a rate of 10 °C/min. The outlet gas composition was continuously monitored by mass spectrometry; typically, NO ($m/e = 30$), NO₂ ($m/e = 46$), N₂O ($m/e = 44$), O₂ ($m/e = 32$), and N₂ ($m/e = 28$) were monitored. The mass spectrometer was calibrated for NO, and therefore quantitative analysis of the desorbed NO was possible. Whenever desorption of NO and NO₂ appeared together, the NO signal was corrected to account for cracking of NO₂ to NO in the chamber. Accordingly, 2.7 times the NO₂ signal was subtracted from the NO signal, in accordance with the literature [48]. Only the corrected NO signals are presented here.

2.6. Temperature-programmed surface reaction (TPSR) tests

TPSR experiments were conducted in the same apparatus as the TPD tests by first adsorbing NO and O₂ on the catalysts and then ramping up the temperature in a flowing gas stream containing CH₄ and O₂. A total of 0.1 g of catalyst was used for TPSR. The adsorption and purging procedure was similar to that for the NO–O₂-TPD described above. The surface reaction was carried out by flowing a mixture of 2% CH₄ and 5% O₂ over the catalyst and increasing the temperature to 700 °C at a rate of 10 °C/min. The following reactants and products were monitored by mass spectrometry: CH₄ ($m/e = 15$), O₂ ($m/e = 32$), NO ($m/e = 30$), NO₂ ($m/e = 46$), N₂/CO ($m/e = 28$), CO₂/N₂O ($m/e = 44$), and H₂O ($m/e = 18$). The m/e ratio of 15 was used for CH₄ to distinguish it from atomic O. Similar to the TPD data, the NO signal was corrected ($2.7 \times \text{NO}_2$ value was subtracted from the NO recorded) when both NO and NO₂ were eluted during TPSR. FTIR gas analysis was used to check for CO production under these conditions, because CO and N₂ are indistinguishable by mass spectrometry (both having $m/e = 28$), and also for distinguishing CO₂ from N₂O. The FTIR apparatus (Mattson, Research Series 1) was equipped with a 0.75 L/5.6 m cell operating at 150 °C. Generally, 100 scans were used to collect the FTIR spectra with a resolution of 4.0 cm⁻¹ and a gain of 4.0. Both the mass spectrometer and FTIR device were calibrated for selected gas components, to quantify the N₂, CO, and CO₂ produced.

Reaction light-off in methane combustion was examined over several catalysts by flowing a mixture of 2% CH₄–5% O₂–He at 50 ml/min and ramping the temperature from room temperature 700 °C at a rate of 10 °C/min. Generally, ~0.1 g

of catalyst was used, after pretreatment in He at 500 °C for 1.5 h. Consumption of CH₄ ($m/e = 15$) and O₂ ($m/e = 32$) was monitored by mass spectrometry, along with production of CO ($m/e = 28$) (after subtracting the amount of CO due to cracking of CO₂ in the chamber), CO₂ ($m/e = 44$), and H₂O ($m/e = 18$). To check the contribution of gas-phase combustion of CH₄, blank tests were performed with an empty reactor at the same conditions.

3. Results and discussion

3.1. Catalyst characterization

Table 1 lists the parent and nitric acid-leached Ag–alumina catalysts examined in this work. Leaching effectively removed all weakly bound silver from the sample. For example, AlAg(0.8,L), a leached sample with 0.8 wt% Ag, was obtained from the parent catalyst AlAg(4.9,CG). Thus, only ~16% of the original silver remained in the sample after leaching. Accompanying the removal of silver, a small decrease in surface area (from 260 to 223 m²/g) was observed in the leached sample, which could be due to the further calcination of the leached catalyst at 650 °C for 3 h. Similarly, AlAg(1.1,L) was obtained from the parent catalyst AlAg(5.8,CG). For the parent catalysts with higher silver loadings, such as AlAg(9.7,CG) and AlAg(21.5,CG), the corresponding leached samples, AlAg(2.6,L) and AlAg(6,L), respectively, retained higher amounts of bound silver. Interestingly, the surface areas of these two leached samples increased compared with the parent catalysts, for example, from 191.4 m²/g in AlAg(21.5,CG) to 222.5 m²/g in AlAg(6,L). Surface area increase may be due to the removal of silver particles blocking pores in the as-prepared Ag–alumina catalysts with high Ag content. A small loss of alumina (3–5 wt%) also occurred on leaching. For comparison, the as-prepared silver-free alumina, Al₂O₃(CG), was treated similarly in nitric acid, and the sample thus obtained is denoted as Al₂O₃(L). The surface area

Table 1
Properties of Ag–alumina catalysts

Sample ^a (Ag, bulk wt%) ^c	BET SA (m ² /g _{cat})	Sample ^b (Ag, bulk wt%) ^c	BET ^c SA (m ² /g _{cat})	Surface ^d Ag content (wt%)
AlAg(4.9,CG)	260.9	AlAg(0.8,L)	223 (171.5)	0.9
AlAg(5.8,CG)	248.6	AlAg(1.1,L)	229.3 (171.3)	0.9
AlAg(9.7,CG)	220.7	AlAg(2.6,L)	230 (175.8)	–
AlAg(21.5,CG)	191.4	AlAg(6,L)	222.5 (200.6)	4.7
Al ₂ O ₃ (CG)	220.6	Al ₂ O ₃ (L)	205.5	–

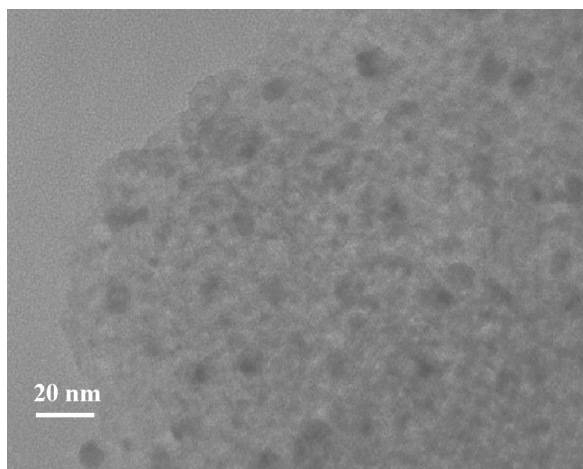
^a Samples in this column are as prepared by cogelation, after air calcination at 650 °C for 5 h.

^b Samples in this column are the corresponding nitric acid leached materials, for example, AlAg(0.8,L) was leached from AlAg(4.9,CG), etc. All leached samples were calcined at 650 °C for 3 h.

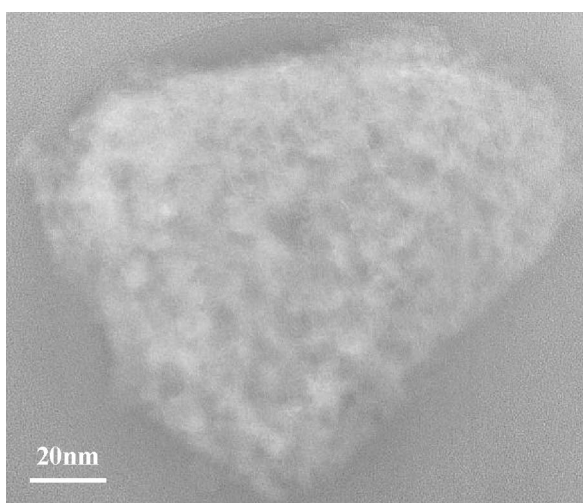
^c The value in the parenthesis is the BET surface area of used sample at the conditions of Fig. 5 at 300–700 °C for ~30 h, except the AlAg(6,L) run at 600 °C for ~14 h.

^d Surface content of silver in the leached samples was measured by XPS.

^e ICP analysis was used to measure the total amount of silver in the parent and leached samples.



(a)



(b)

Fig. 1. HRTEM of (a) AlAg(4.9,CG); (b) nitric acid-leached AlAg(0.8,L) after calcination in air at 650 °C.

of Al₂O₃(L) was 205.5 m²/g, compared with 220.6 m²/g for Al₂O₃(CG).

The surface composition of the leached catalysts was examined by XPS, and results are compared with the bulk composition obtained by ICP, as shown in Table 1. Clearly, the surface concentration of Ag is very close to that in the bulk for the leached samples, AlAg(0.8,L), AlAg(1.1,L), and AlAg(6,L). Bulk analysis was done by ICP. These findings suggest that silver is well dispersed in Ag–alumina catalysts, prepared by the coprecipitation-gelation method used in this work.

A HRTEM picture of a pair of parent and leached Ag–alumina catalysts is shown in Fig. 1. Fig. 1a shows the parent sample AlAg(4.9,CG). Silver particles <10 nm in size are observed in good contact with the alumina matrix. After nitric acid leaching, no particles remained on the leached sample, AlAg(0.8,L), as shown in Fig. 1b.

XRD was performed to identify the crystalline phases present in the Ag–alumina catalysts. Fig. 2 shows the results for the alumina (both as-prepared and nitric acid-treated), leached AlAg(0.8,L), and AlAg(7.7,L) samples, and one as-prepared high-Ag-content sample AlAg(11,CG). For comparison, XRD

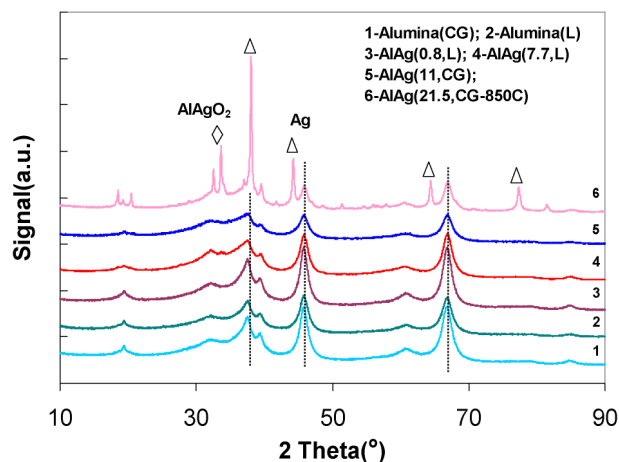


Fig. 2. XRD of alumina and Ag–alumina catalysts after calcination in air at 650 °C.

was also used to analyze the other high-silver-content catalyst, AlAg(21.5,CG-850), which was calcined at 850 °C for 5 h in an attempt to form silver aluminate [44]. As can be seen in Fig. 2, strong diffraction lines due to metallic silver ($2\theta \approx 38.1^\circ$, 44.3° , 64.5° , 77.6°) and silver aluminate ($2\theta \approx 33.7^\circ$) were observed in AlAg(21.5,CG-850C) (line 6), and the silver particle size was calculated as 30.5 nm. Thus, the high-temperature calcination (850 °C) and high silver loading causes agglomeration of silver particles, in comparison with the <10 nm silver nanoparticles shown in Fig. 1a for AlAg(4.9,CG). The crystallite size of alumina was calculated as ~ 5 nm based on peaks at $2\theta \approx 45.8^\circ$ and 66.8° [49]. For the two leached Ag–alumina samples, and even for AlAg(11,CG), the diffraction peaks were due only to the alumina phase (indicated by the dotted lines), and no metallic Ag was identified in these samples. However, a weak new peak appeared at $2\theta \approx 33^\circ$ for AlAg(7.7,L) which is assigned to silver aluminate [44,49]. Some new features also appear around the peaks of alumina at 20° and 60° , where lines due to silver aluminate also exist. Because the carrier alumina is of small crystallite size, it exhibits broad diffraction peaks at these positions, making it difficult to discern peaks due to silver aluminate. In the case of the AlAg(0.8,L) sample, even though no silver aluminate lines were detected, this may be due to the small amount of silver and high dispersion. Silver aluminate has been proposed as an active species for SCR in the literature [22,23,44].

To further examine the oxidation states of silver in leached Ag–alumina catalysts, XPS was carried out with three leached samples, AlAg(0.8,L), AlAg(1.1,L), and AlAg(2.6,L). For comparison, XPS was also performed on an as-prepared Ag–alumina sample, AlAg(4.9,CG). The XP spectra are shown in Fig. 3, which also lists the binding energies of Ag 3d_{5/2} on these samples. The binding energy of Ag 3d_{5/2} (at ~ 368.0 eV) does not shift much among the leached catalysts and the parent catalyst. The binding energies of Ag⁰ and Ag₂O are 368.3 and 367.5 eV, respectively [25,50]. It is hard to assign the BE values shown in Fig. 3 to either metallic silver or oxidized silver, because a more complex electronic environment may be considered a result of the co-gelation preparation (i.e., silver

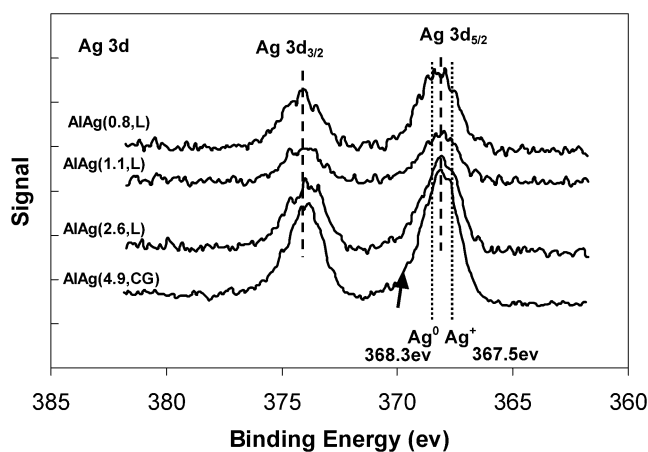


Fig. 3. XPS of leached and as prepared Ag–alumina catalysts; binding energy of Ag $3d_{5/2}$: AlAg(0.8,L) 368.1 eV; AlAg(1.1,L) 368.0 eV; AlAg(2.6,L) 367.9 eV; AlAg(4.9,CG) 368.0 eV.

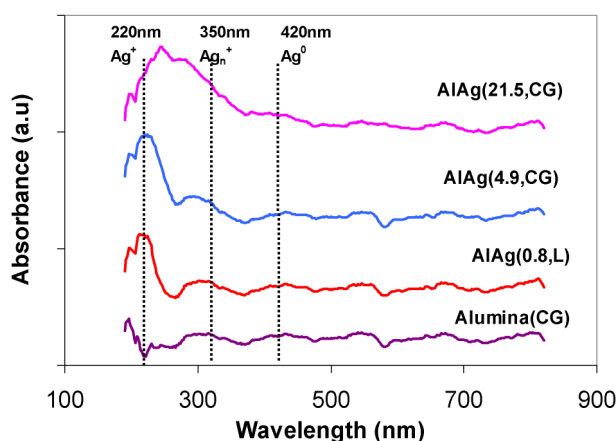


Fig. 4. UV–vis DRS of as prepared alumina and Ag–alumina catalysts; at RT in air.

aluminate species). Seker et al. [46] reported two main peaks of Ag $3d_{5/2}$ at 370.6 and 372.0 eV (C 1s at 284 eV) for their Ag–alumina samples prepared by a sol–gel technique. The type of silver species was not identified in that work either, due to the relatively high BE values, which indicated strong electronic interaction with the alumina.

We further explored the oxidation state of silver in our samples using UV–vis DRS. As shown in Fig. 4, UV–vis analysis demonstrates the existence of different oxidation states of silver. All of the spectra are shown just as obtained. AlAg(0.8,L) had been used under reaction conditions before the analysis, whereas the other samples were as-prepared. Compared with alumina, a significant new peak appears at 220 nm for both the leached AlAg(0.8,L) and parent AlAg(4.9,CG), which is assigned to Ag^+ [23,41]. For the latter sample, there is also a small peak at 350 nm, assigned to oxidized silver clusters ($Ag_n^{\delta+}$), and this feature is still apparent after subtraction of the alumina baseline. With higher silver amounts, such as in AlAg(21.5,CG), besides Ag^+ (220 nm), a broad peak appears at 290–350 nm ($Ag_n^{\delta+}$), as well as a weak peak at ~ 420 nm (Ag^0) [23,41]. This can be explained by the presence of silver nanoparticles and clusters covered by oxygen (in air), and

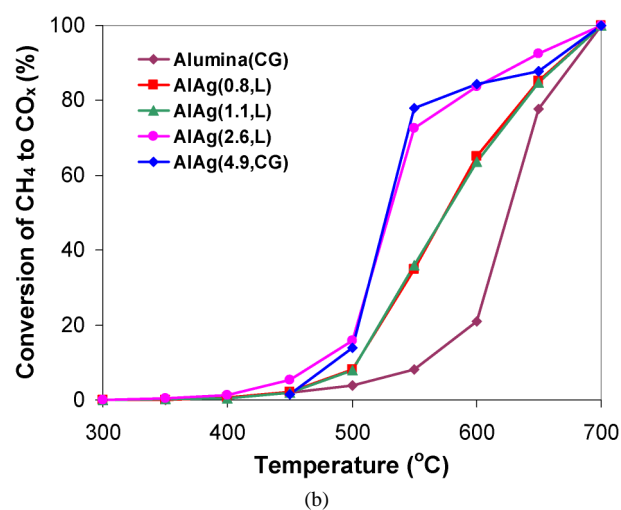
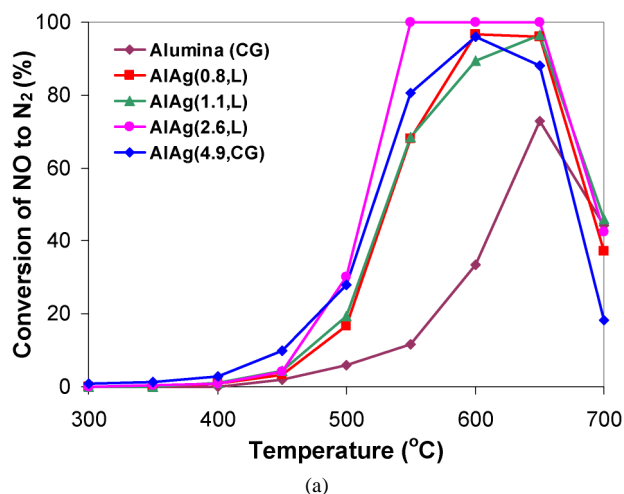


Fig. 5. Selective catalytic reduction of NO with CH_4 over alumina and Ag–alumina catalysts. (a) Conversion of NO to N_2 ; (b) conversion of CH_4 to CO_x . Feed gas: 0.25% NO–2% CH_4 –5% O_2 /He; SV = 9000 h^{-1} .

hence the band due to $Ag_n^{\delta+}$ grows stronger, but not the band due to Ag^0 . It is also noteworthy that even for the high silver-content sample, AlAg(21.5,CG), the color is surprisingly light and still off-white. Hence, in the Ag–alumina catalysts as prepared in this work, silver is highly dispersed and exists mainly as isolated silver ions, possibly embedded in the alumina, [Ag–O–Al], and oxidized silver nanoparticles. Furthermore, the stability of the [Ag–O–Al] species in the SCR reaction conditions is excellent, as can be seen by the spectra of the used AlAg(0.8,L).

3.2. SCR of NO with CH_4 over Ag–alumina

Fig. 5 shows the conversion of NO to N_2 and CH_4 to CO_x over the leached Ag–alumina catalysts at 300–700 °C. The figure also shows the results from tests with silver-free Al_2O_3 and one parent catalyst, AlAg(4.9,CG). Over Al_2O_3 (CG), NO reduction begins at 450 °C and reaches a maximum conversion to N_2 of 70% at 650 °C. This alumina is a poor CH_4 -SCR catalyst. High surface area alumina has been reported to be an active catalyst for the SCR of NO with propene/propane or oxygenates [48,51]. Burch et al. [48] reported a peak NO to N_2

conversion of $\sim 80\%$ at 550°C for C_3H_8 -SCR of NO over γ -alumina at C:N ratio of 6 and space velocity of $18,000\text{ h}^{-1}$. Meunier et al. [51] found that the maximum NO conversion (60%) was reached at 600°C in propene SCR, and that adding a small amount of silver (1.2 wt%) caused no significant change in activity, even though it shifted the active temperature window to slightly lower values. Kung et al. [23] also pointed out the important role of alumina sites for SCR of NO in a proposed bifunctional mechanism, with metal ions as sites for NO_2 or adsorbed nitrate formation and alumina providing sites for dinitrogen formation.

With the addition of 0.8 wt% Ag in alumina, as in the sample AlAg(0.8,L), the conversion maximum of NO to N_2 shifts to 600°C and reaches 95%. AlAg(0.8,L) and AlAg(1.1,L) show very similar conversions of NO and CH_4 . When the silver content increases, such as in AlAg(2.6,L), a higher conversion of NO and a wider active temperature window are observed, with NO to N_2 conversion reaching $\sim 100\%$ at $550\text{--}650^\circ\text{C}$. The conversion of NO to N_2 is similar over the pair of leached and parent catalysts, AlAg(0.8,L) and AlAg(4.9,CG), as shown in Fig. 5a. However, the parent catalyst shows much higher conversion of CH_4 (Fig. 5b), i.e. 78% compared to 36% for the leached material at 550°C . The lower conversion of CH_4 is attributed to the absence of silver particles on AlAg(0.8,L), which is consistent with literature reports of metallic silver nanoparticles catalyzing the direct CH_4 combustion reaction [22–26,29,41,42]. Hence, leaching enhances the catalyst selectivity toward CH_4 oxidation by NO_x .

3.3. Surface adsorption of NO/O₂ and reactivity with CH₄

3.3.1. NO–O₂-TPD

The surface interaction of NO and O₂ with alumina or Ag/alumina catalysts has been reported to play an important role in the mechanism of SCR of NO by hydrocarbons through the formation of adsorbed species, such as nitrites or nitrates [27,29,48,51–55]. Formation of surface nitrates has been found by FTIR spectra over both alumina [51–53] and Ag/alumina [27,29,51,54,55] catalysts after adsorption of NO and O₂. TPD is also useful because it probes different surface structures by monitoring the species desorbed over the range of temperature of interest to catalysis [48,54]. Therefore, in this work NO–O₂-TPD was performed over alumina and leached and as-prepared Ag–alumina samples to identify the types of surface adsorption sites of different structures and elucidate their relevance for the catalysis of the NO reduction by CH_4 .

3.3.1.1. NO–O₂-TPD in He NO–O₂-TPD results are shown in Figs. 6 and 7 for desorption in flowing He gas. Analysis of the desorbed species was done by mass spectrometry. Signals due to O₂ ($m/e = 32$), NO ($m/e = 30$), and NO₂ ($m/e = 46$) were detected. No N_2O ($m/e = 44$) or N_2 ($m/e = 28$) was observed, in agreement with previous reports for NO–O₂-TPD over alumina [48] and Ag–alumina [54]. For most of the data reported here, replicate tests were performed. The TPD-mass spectrometry technique is very stable, and reproducible results were obtained.

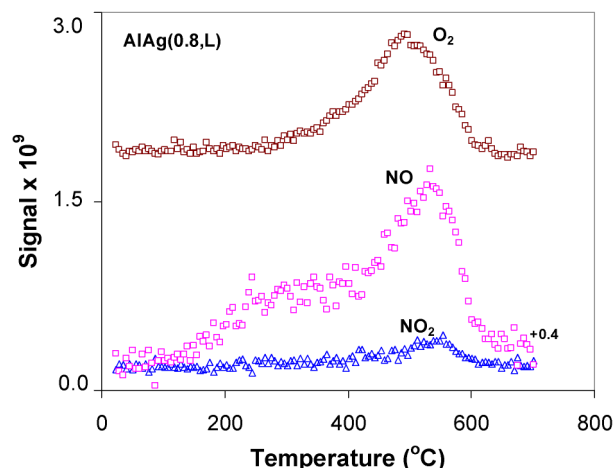
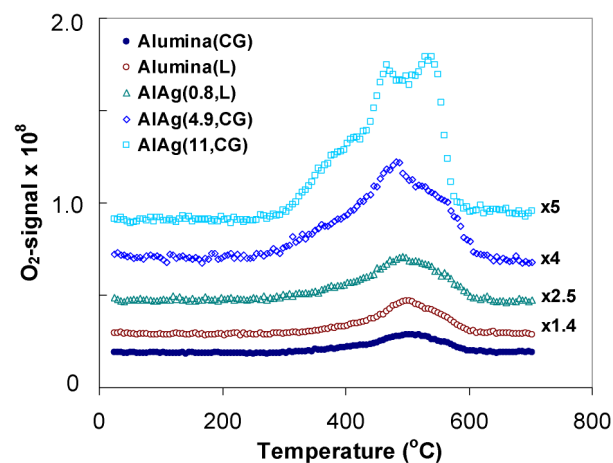


Fig. 6. NO–O₂-TPD in He from AlAg(0.8,L).

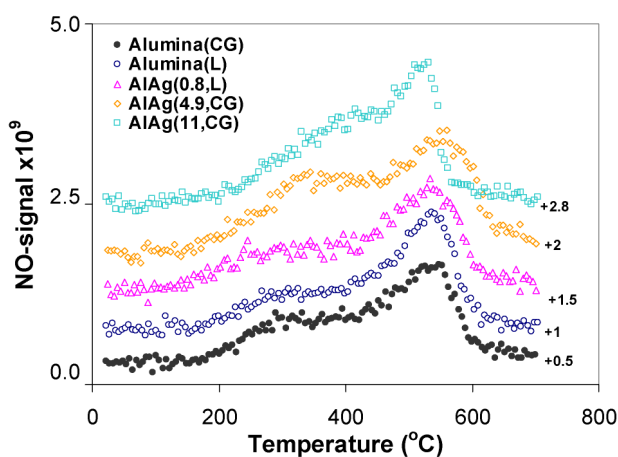
Fig. 6 shows the TPD profiles from the leached AlAg(0.8,L) sample. Desorption of O₂ starts at around 300°C , peaks at 497°C , and levels off at $\sim 620^\circ\text{C}$. No production of N_2O or N_2 is found over the whole temperature range. Two desorption peaks of NO are observed, with the first beginning at 170°C and peaking at 300°C , followed by a second peak with a maximum at 539°C . A NO₂ peak is also observed at 539°C . Therefore, the NO peak at 539°C is accompanied by NO₂ and O₂ desorption. Kameoka et al. [54] reported similar TPD features over a 2 wt% Ag/alumina. In their case, two NO desorption peaks were observed, one at low temperature (250°C) and the other at high temperature (480°C). The latter peak was accompanied by O₂ and NO₂ desorption. Based on their FTIR results (NO–O₂ adsorption and then heating in He), these authors assigned three types of surface nitrates on Ag/alumina with thermal stability in the order monodentate > bidentate > bridging-nitrates (NO_3^-). Hence, the desorption peaks at 539°C in Fig. 6 may be assigned to decomposition of nitrate species, whereas the NO desorbed at low temperature ($<300^\circ\text{C}$) must be due to weakly bound NO, because neither O₂ nor NO₂ is observed accompanying this peak.

To elucidate the role of silver sites and alumina sites in adsorption of NO/O₂, similar TPD tests were also conducted over bare alumina (both as-prepared and acid-treated) and the silver-containing alumina samples. The desorption patterns are shown in Figs. 7a–7c for O₂, NO, and NO₂, respectively. As can be seen from these figures, the TPD profiles from alumina and AlAg(4.9,CG) are in good correspondence with those over AlAg(0.8,L), as described above for Fig. 6. Briefly, a similar main desorption peak for both NO and NO₂ is seen at 539°C in all three samples. The results indicate that silver does not modify the alumina surface, and that the surface nitrate species are bound on the alumina sites rather than on silver.

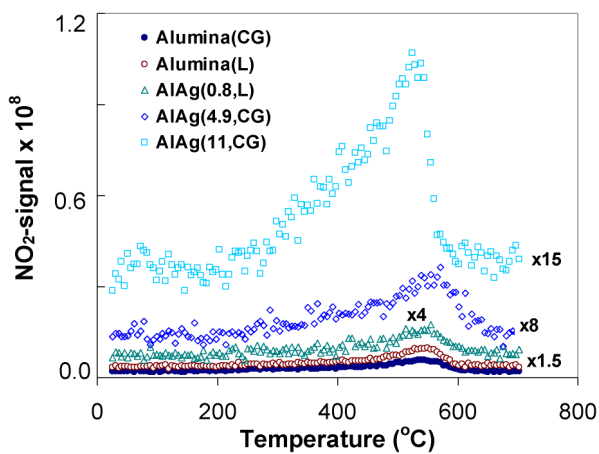
To probe the effect of adding more silver onto the alumina, a sample with higher silver content (11 wt%), AlAg(11,CG), was also examined; the results are shown in Fig. 7. For this sample, NO begins to desorb from 170°C and continues up to 400°C , while the second peak is still present, with a maximum slightly shifted to 529°C (vs. 539°C). Thus, the TPD of NO is similar to that of the other samples, except that an en-



(a)



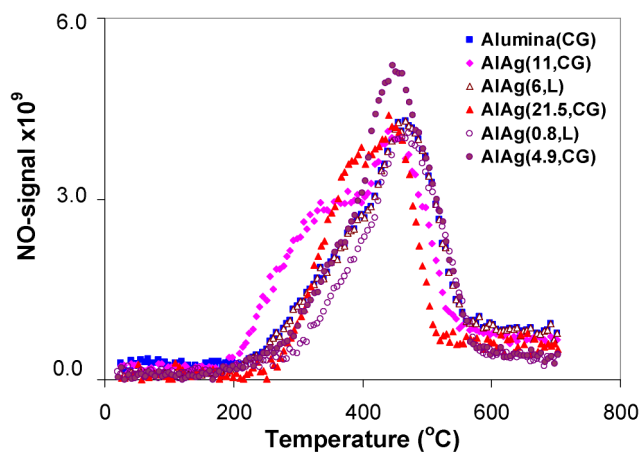
(b)



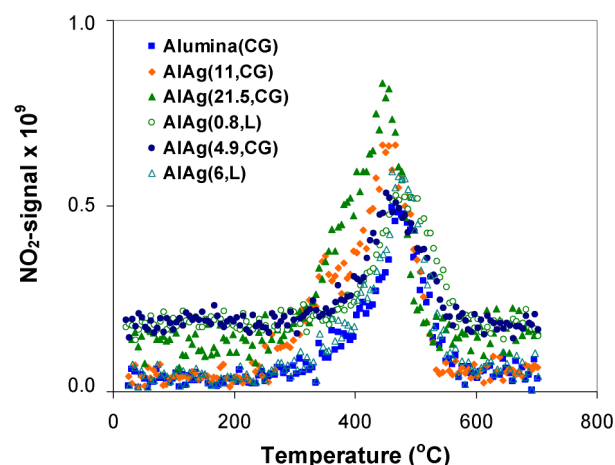
(c)

Fig. 7. NO–O₂-TPD in He from alumina and silver–alumina catalysts: (a) O₂; (b) NO; (c) NO₂.

hanced NO adsorption is shown over the low-temperature range over AlAg(11,CG). This is attributed to NO adsorbed on the silver nanoparticles, which are present in this sample but absent from alumina or AlAg(0.8,L). Using peak deconvolution (PeakFit V4.12; Seasolve Software), we found that the low-temperature peak comprises 21.9–30% of the total desorbed NO from Al₂O₃(L or CG) and AlAg(0.8,L), whereas it is 37.6% of the NO desorbed from AlAg(4.9,CG). With even higher Ag



(a)



(b)

Fig. 8. NO–O₂-TPD in 5% O₂/He: (a) NO; (b) NO₂.

loading (e.g., for the AlAg(11,CG) sample), the percentage of NO desorbed at low temperature increases to 50%, indicating a greater contribution of the Ag nanoparticles. Quantitatively, the total amount of desorbed NO over the whole temperature range was close among all these catalysts, 0.9–1.1 μmol/m². Thus, no significant effect of silver loading is observed. Earlier, Kameoka et al. [54] found no major NO adsorption difference between a 2 wt% Ag/Al₂O₃ and Al₂O₃ by TPD and DRIFTS measurements, but did not examine the potential effect of higher silver loadings. Meunier et al. [51] proposed that increasing the loading of silver (2–10 wt%) on alumina promotes NO/O₂ adsorption based on in situ DRIFTS and thermogravimetric analyses.

3.3.1.2. NO–O₂-TPD in O₂ Although TPD is generally run in inert gas streams, such as helium, it is also important to consider the effect of a reactive sweep gas. Thus, in this work TPD was also performed in a 5% O₂/He gas mixture to simulate the lean-burn conditions in practical SCR systems. The results, shown in Fig. 8, indicate that, similar to TPD in He, no N₂ or N₂O was identified in the desorbed gases. However, in contrast to TPD in He, no O₂ desorption occurred. Figs. 8a and 8b show the TPD profiles of NO and NO₂ from alumina, leached AlAg(0.8,L) and its parent AlAg(4.9,CG), another leached sample with

Table 2
N₂, CO₂, and NO eluted during TPSR^a and TPD^{a,b}

Sample	Amount of N ₂ produced (μmol/m ² _{cat})	Amount of CO ₂ produced (μmol/m ² _{cat})	NO (TPSR) (μmol/m ² _{cat})	NO (TPD) (μmol/m ² _{cat})
Al ₂ O ₃	–	53.6	1.0	1.2
AlAg(0.8,L)	–	152.5	0.8	1.3
AlAg(4.9,CG)	–	819	1.2	1.5
AlAg(21.5,CG)	0.34	2982.6	1.0	1.7

^a In the temperature range 25–700 °C; measured by mass spectrometry.

^b In O₂/He gas mixture.

6 wt% Ag, AlAg(6,L), and two Ag–alumina samples with relatively high Ag loadings, AlAg(11,CG) and AlAg(21.5,CG). For alumina, NO desorption starts at 200 °C, peaks at 460 °C, and then levels off at 600 °C. A similar trend was observed for AlAg(0.8,L), with the desorption peak also positioned at 460 °C. For the parent catalyst AlAg(4.9,CG), desorption of NO also begins at 200 °C and levels off at 600 °C, even though the peak is slightly shifted to 450 °C and the peak intensity is slightly increased. The amount of NO desorbed from the above three samples was 1.2–1.5 μmol/m², as shown in Table 2. A similar desorption pattern is also observed for AlAg(6,L) with a major peak at 460 °C and desorbed NO of 1.6 μmol/m². Comparing these catalysts, we assign the desorption feature with a peak at ~460 °C to NO_x species adsorbed on alumina sites. As before, these TPD data also show that the alumina-bound ionic silver species [Ag–O–Al] do not modify the adsorption properties of alumina surface.

As shown in Fig. 8, the high-silver-content samples, AlAg(11,CG) and AlAg(21.5,CG), have exaggerated low-temperature desorption. Peak deconvolution performed for all of the TPD profiles of Fig. 8a shows a small NO desorption peak with maximum at 320–350 °C accounting for 11–18% of the total desorbed NO from the alumina, leached Ag–alumina, and AlAg(4.9,CG) samples. However, this value increases to 30–45% of the total NO desorbed for the samples AlAg(11,CG) and AlAg(21.5,CG), which corresponds very well with the data of Fig. 7. Relatively high total NO desorption (1.7 μmol/m²) is reported in Table 2 for AlAg(21.5,CG), attributed to the additional low-temperature adsorption of NO_x on the oxidized surface of silver nanoparticles.

3.3.2. TPSR tests

In previous work, the reactivity of surface species formed after adsorption of NO/O₂ with various hydrocarbons or oxygenates, such as propene/propane [27,48,51,53–56], higher hydrocarbons (C₄–C₈) [29,56], and ethanol/methanol [48,54], has been examined over alumina [48,51,53] and silver/alumina [27,29,51,54–56] catalysts by FTIR or TPR measurements. Consistently, different research groups have reported high reactivity of adsorbed NO_x species to these reductants, confirming these species importance as intermediates for the SCR of NO. However, to our knowledge, no such information is available for the reactivity of adsorbed NO_x species with CH₄ over alumina or Ag/alumina catalysts. Consequently, in this work TPSR tests were performed by flowing CH₄/O₂ over the alu-

mina and silver–alumina samples after they were exposed to co-adsorption of NO/O₂. The TPSR results are compared among catalysts with different structures (i.e., blank alumina, silver particle–free leached Ag–alumina, and silver particle–laden Ag–alumina with high silver content).

Figs. 9a–9e presents the TPSR results over Al₂O₃(CG), AlAg(0.8,L), AlAg(4.9,CG), and AlAg(21.5,CG). The spectra were repeated twice for each sample, and reproducible TPSR results were obtained. In Fig. 9a, the top part shows the profiles of O₂ signal for the above four samples, and the bottom part shows the CH₄ profiles. As indicated by the dotted line a, over AlAg(21.5,CG), consumption of O₂ and CH₄ first appears at 430 °C, followed by a much faster consumption after 460 °C. For AlAg(4.9,CG), these two temperatures shift to higher values, as shown by the dotted line b at 510 and 578 °C, respectively. Similar profiles are observed over AlAg(4.9,CG) and AlAg(0.8,L), although the consumption of O₂ and CH₄ is weaker for the latter, which could be due to the absence of silver particles. Alumina exhibits an even weaker consumption of the two reactants.

Accompanying the consumption of O₂ and CH₄, *m/e* signals of 28 for N₂/CO and 44 for CO₂ were produced, as well as desorption of NO/NO₂, as shown in Figs. 9b and 9c. It should be pointed out that no N₂O was produced over these samples, as verified by FTIR gas analysis. Hence the mass signal of 44 was assigned to CO₂ only. The *m/e* = 28 signal is more difficult, however, because it can be due to both N₂ and CO. Two sources of CO are considered: (1) CO from the cracking of CO₂ in the mass spectrometer (at 12% of total CO₂ [57]) and (2) CO produced during TPSR. For the first effect, the raw data were corrected by subtracting this part CO from signal *m/e* = 28 in Fig. 9b. To check for the second effect, CO was monitored by on-line FTIR; the results are presented in Fig. 9d. As this figure shows, CO is produced from Al₂O₃(CG) and leached AlAg(0.8,L) in the temperature range 345–700 °C, with the amount of CO increasing with increasing temperature, reaching 333 ppm for Al₂O₃(CG) and 300 ppm for AlAg(0.8,L) at 700 °C. Thus, partial oxidation of CH₄ occurs on these two catalysts. Over AlAg(4.9,CG), however, much less CO is produced compared with the former two catalysts. This means that the presence of silver particles is beneficial to burning off the CO produced. In view of Fig. 9d, in Fig. 9b, the *m/e* = 28 signal is denoted as N₂/CO for Al₂O₃(CG), leached AlAg(0.8,L), and AlAg(4.9,CG). For AlAg(21.5,CG), the *m/e* = 28 signal is assigned to N₂ only. Also note that no reduced nitrogen-containing products, such as NH₃ and HCN, accompany the CO production during TPSR, as checked by IR.

Similar to the NO–O₂–TPD results (Fig. 8), NO starts to desorb at ~200 °C during TPSR (Fig. 9b). Along with the NO desorption, NO₂ desorption was also observed; the NO₂ levels produced were measured separately by FTIR, as shown in Fig. 9e. The peak positions of desorbed NO₂ by both mass spectrometry and FTIR are consistent between Figs. 9b and 9e. Although the NO₂ level decreases with temperature above 460 °C, Fig. 9e shows that NO₂ (500 ppm) is present in the gas even at 700 °C. Over AlAg(21.5,CG), the *m/e* = 28 signal starts to increase from 300 to 400 °C as a small peak, then in-

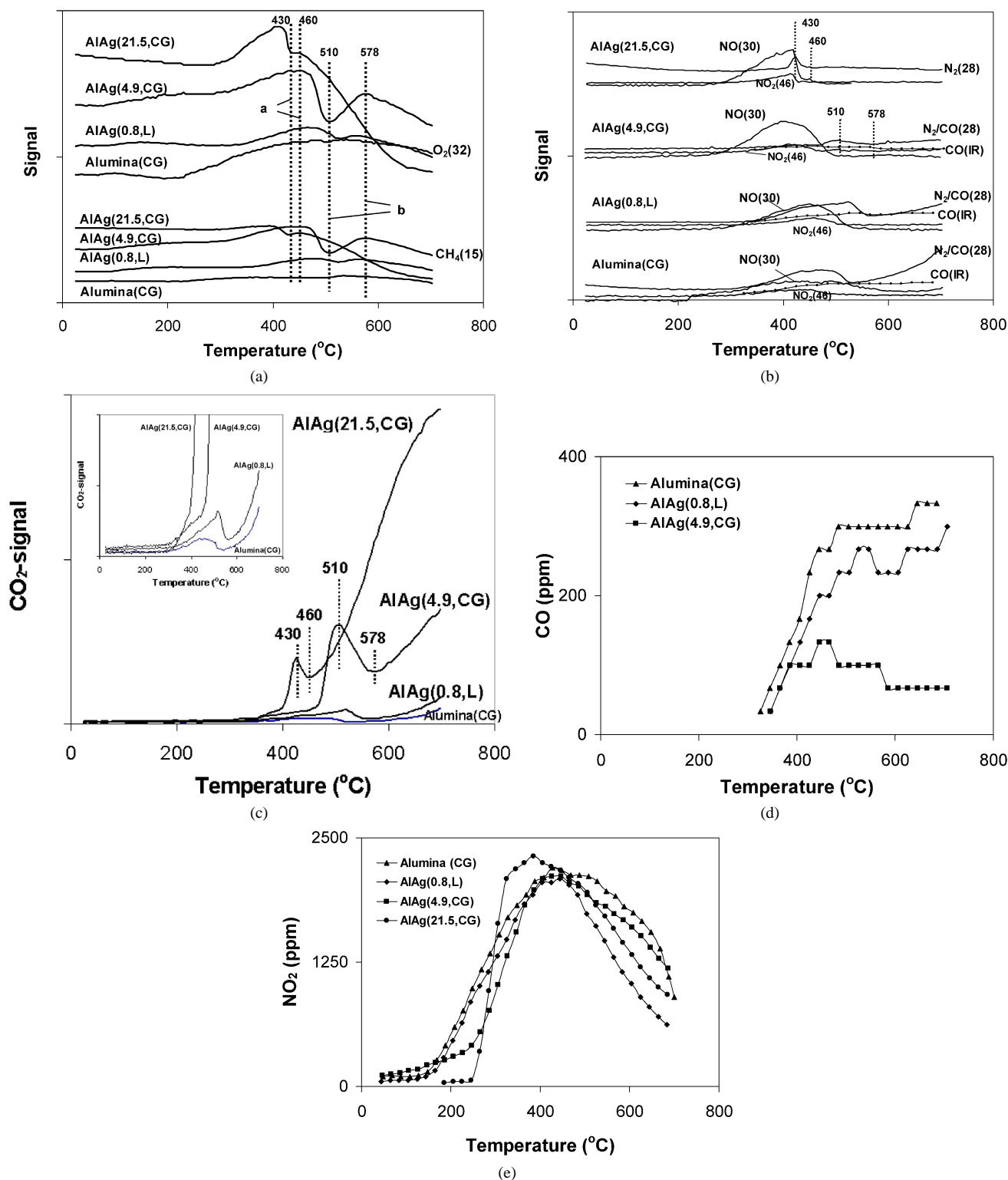


Fig. 9. TPSR in CH₄/O₂, over alumina and Ag–alumina catalysts pre-exposed to NO–O₂: (a) O₂ and CH₄; (b) NO, NO₂, N₂/CO and CO(IR); (c) CO₂; (d) CO and (e) NO₂ profile measured by FTIR. In (b), the NO₂ signal was scaled up 2× for alumina, AlAg(0.8,L) and AlAg(4.9,CG) due to the weak signal. The inset in (c) highlights the CO₂ signal at low temperatures.

creases sharply and peaks at 430 °C and then decreases slowly; it is still measurable at 700 °C. For the $m/e = 28$ signal over AlAg(4.9,CG), there is also a broad peak at 300–450 °C, and a peak at 510 °C. The profiles for $m/e = 28$ are similar for Al₂O₃(CG) and AlAg(0.8,L). For AlAg(0.8,L), the $m/e = 28$

signal begins to increase at 320 °C, peaks at 523 °C and then reaches a valley at 570 °C, however, above 570 °C, the signal keeps going up with temperature. A similar two-stage pattern is also found for the Al₂O₃(CG) sample, with the peak at 470 °C and the valley at 540 °C. For the latter three samples, the

$m/e = 28$ signal may comprise both N_2 and CO, as revealed by independent FTIR gas analysis for CO in Fig. 9d. Accordingly, the mass signals of CO corresponding to Fig. 9d are also shown in Fig. 9b, denoted as CO(IR), over AlAg(4.9,CG), Al_2O_3 (CG), and AlAg(0.8,L). The net N_2 production can be obtained by subtracting the CO(IR) from the $m/e = 28$ signal; this subtraction has no significant effect on the $m/e = 28$ profile. Hence, N_2 production continues at high temperatures (up to 700 °C), although the extent is strongly affected by the methane combustion activity of each catalyst and the corresponding availability of methane. (As shown in Fig. 9a, very little methane remains over the AlAg(21.5,CG) material at 700 °C.) On all samples, temperatures above ~300 °C are necessary to initiate the CH_4 activation via adsorbed NO_x species for N_2 production.

TPSR profiles of CO_2 are shown in Fig. 9c. The light-off temperature is 300 °C for CO_2 production over all four samples, the same as the light-off temperature for N_2/CO shown in Fig. 9b. Apparently, much stronger CO_2 production occurs over AlAg(21.5,CG) than over the other samples with lower silver loading or without silver. Comparing the leached AlAg(0.8,L) and parent AlAg(4.9,CG), it is clear that removing silver particles suppresses the direct CH_4 oxidation to CO_2 , whereas the CO_2 production over AlAg(0.8,L) is slightly higher than that over Al_2O_3 (CG).

Furthermore, the TPSR profiles of $m/e = 28$ and 44 (CO_2) for each catalyst are in total correspondence with the profiles of CH_4 and O_2 . For example, a peak and a valley are seen for N_2/CO and CO_2 in Figs. 9b and 9c at exactly the same temperatures as for CH_4 and O_2 in Fig. 9a, 430 and 460 °C for AlAg(21.5,CG) and 510 and 578 °C for AlAg(4.9,CG), respectively, as represented by the dotted lines in Figs. 9b and 9c. Shi et al. [58] observed a very similar two-stage profile of CH_4/O_2 consumption and accompanying N_2/CO_2 production during TPSR in a CH_4-O_2 stream after coadsorption of NO/O_2 over an Ag-ZSM-5 catalyst. The light-off temperature for CH_4 consumption and N_2/CO_2 production was reported to be around 350 °C, and Shi et al. proposed that CH_4 reacted with surface nitrates by SCR before reaction with oxygen by direct combustion.

The TPSR results of Fig. 9 also reflect the structural effect of silver in Ag–alumina catalysts. From the CO_2 production shown in Fig. 9c, the CH_4 combustion-dominated range shifted by ~120 °C to lower temperature over AlAg(21.5,CG) compared with the other samples. The high combustion activity of this sample is attributed to the presence of oxygen-covered silver particles [42] as shown on UV–vis (Fig. 4). Further, comparing the leached AlAg(0.8,L) and parent AlAg(4.9,CG) samples, with similar TPSR, the similarity can be attributed to the existence of [Ag–O–Al] species dominant in both samples, as also shown by UV–vis (Fig. 4). However, Fig. 9c shows much lower CO_2 on AlAg(0.8,L) than on AlAg(4.9,CG), due to the absence of silver particles on the leached catalyst, verified by TEM in Fig. 1b.

Table 2 compares the amounts of N_2 and CO_2 eluted in TPSR. For all of the data presented in this table, the values were obtained by integrating from room temperature to 700 °C. For the samples that produce CO during TPSR, ob-

taining the amount of N_2 from the $m/e = 28$ signal is difficult, and so the numbers are not shown. The desorbed NO was also calculated and compared with the NO desorbed during TPD in O_2 (Fig. 8). The difference between these two NO values should indicate the part of NO consumed during TPSR; for example, over AlAg(21.5,CG), the difference in NO is 0.7 $\mu\text{mol}/\text{m}^2$, corresponding to 0.35 $\mu\text{mol}/\text{m}^2$ of N_2 produced (based on stoichiometry), very close to the measured amount of N_2 (0.34 $\mu\text{mol}/\text{m}^2$) produced during TPSR. The trend of CO_2 values show that the presence of silver particles enhances CO_2 production by the direct methane oxidation reaction.

3.3.2.1. Transient methane combustion tests Separate tests with CH_4 and O_2 were conducted to examine the surface activation of CH_4 without first adsorbing $NO-O_2$ (nitrates). The CO_2 profiles produced are shown in Fig. 10. To check for the possibility of gas-phase reaction, a blank test was run with an empty reactor (as shown in Fig. 10) in which only a trace amount of CO_2 (44) was detected above 600 °C. Therefore, CH_4 is not thermally activated at temperature below 600 °C in the presence of O_2 .

Fig. 10 also shows the CO_2 profiles obtained over alumina and three leached samples, AlAg(0.8,L), AlAg(2.6,L), and AlAg(6,L). CO_2 production starts at ~500 °C over alumina and AlAg(0.8,L) and shifts slightly to ~480 °C for AlAg(2.6,L) and AlAg(6,L). The presence of silver particles promotes the light-off for CO_2 at 400 °C in AlAg(4.9,CG) and 300 °C in AlAg(21.5,CG). Kundakovic et al. [42] reported light-off values of 300, 350, and 500 °C for CH_4 oxidation over Ag particles (7.9 wt% Ag/ZrO₂), Ag clusters (Ag(83)-ZSM-5) and isolated silver ions (Ag(16)-ZSM-5), respectively, in steady-state tests. Table 3 gives the amounts of CO_2 produced for alumina and Ag–alumina catalysts. Comparing AlAg(0.8,L) and alumina indicates that the presence of Ag^+ enhances CO_2 production. Further, the amount of CO_2 produced also increases with an increasing amount of silver ions in the leached catalysts, following the order AlAg(6,L) > AlAg(2.6,L) > AlAg(0.8,L). Much more CO_2 was produced for the two as-prepared catalysts, AlAg(4.9,CG) and AlAg(21.5,CG), apparently due to the presence of silver nanoparticles.

Combining the transient reaction results (Fig. 10) and TPSR (Fig. 9) demonstrates that adsorbed nitrates shift the CH_4 activation temperature to 300 °C during TPSR, especially for alumina and leached Ag–alumina catalysts. We postulate that for all catalysts, adsorbed surface nitrates are essential for CH_4 activation at temperatures as low as 300 °C with concomitant production of N_2 . In contrast, for Ag–alumina catalysts covered with silver nanoparticles, methane can be activated directly by adsorbed oxygen, so that methane combustion begins at 300 °C. However, preadsorbed NO_x on the silver particles does not appear to contribute to N_2 formation at this temperature. As will become clear in what follows, all N_2 produced in the CH_4 -SCR of NO comes from the reaction of NO_x adsorbed on the alumina sites only.

Table 3 also gives the amounts of CO produced for the above samples during transient CH_4-O_2 reaction. For alumina and all three leached samples, CO accompanies CO_2 production.

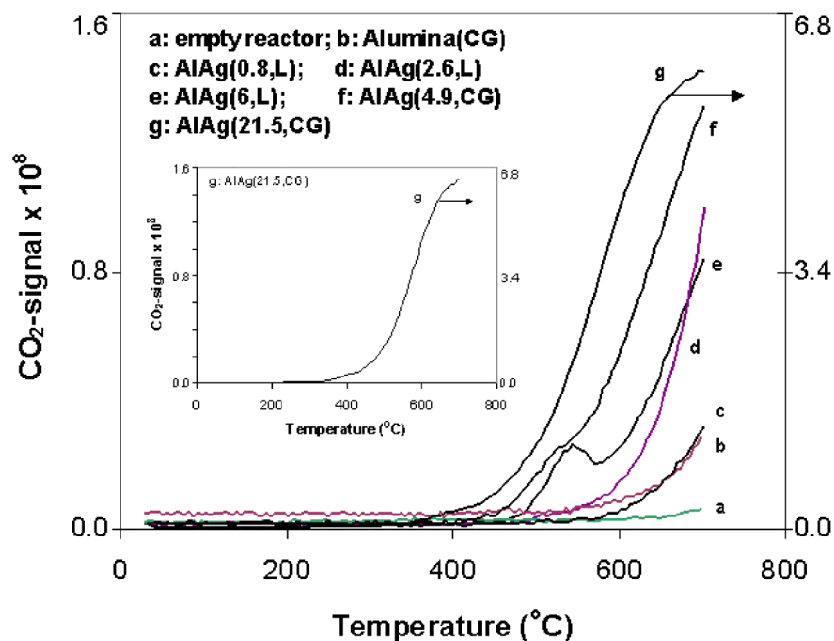


Fig. 10. CO_2 produced during transient $\text{CH}_4\text{-O}_2$ reaction over alumina and Ag–alumina samples from RT to 700°C . The inset highlights the CO_2 signal over AlAg(21.5,CG) (line g).

Table 3
Gaseous products of the $\text{CH}_4\text{-O}_2$ reaction^a

Sample	Amount of CO_2 produced ($\mu\text{mol}/\text{m}_{\text{cat}}^2$)	Amount of CO produced ($\mu\text{mol}/\text{m}_{\text{cat}}^2$)
Al_2O_3	37.9	48.3
AlAg(0.8,L)	49.7	31.4
AlAg(2.6,L)	149	51.1
AlAg(6,L)	196	10.2
AlAg(4.9,CG)	363	0
AlAg(21.5,CG)	1840	0

^a Measured by mass spectrometry during transient tests at the conditions of Fig. 10.

However, for the two as-prepared catalysts, AlAg(4.9,CG) and AlAg(21.5,CG), no CO production is observed over the whole temperature range, again attributed to the presence of silver particles in these samples.

3.3.3. Kinetics of $\text{CH}_4\text{-SCR}$

Kinetics measurements were made over alumina (CG), two pairs of leached and parent Ag–alumina catalysts [AlAg(0.8,L) vs. AlAg(4.9,CG) and AlAg(6,L) vs. AlAg(21.5,CG)], and one leached sample from an 850°C -calcined parent, AlAg(7.5, L-850P). Rates of NO to N_2 and overall rates of CH_4 to CO_x were typically measured at $425\text{--}525^\circ\text{C}$. The gas composition used was of C:N = 1 (0.5% NO–0.5% CH_4 –5% O_2). Some data points were measured at temperatures of $550\text{--}600^\circ\text{C}$ and gas composition of C:N = 5 (0.2% NO–1% CH_4 –7.5% O_2) for AlAg(0.8,L) and AlAg(6,L). Blank tests were also run with the empty reactor at the above temperature range and gas composition conditions. No reaction occurred in the gas phase alone at the above conditions.

Arrhenius-type plots of the rates of $\text{CH}_4\text{-SCR}$ of NO_x are illustrated in Fig. 11. Fig. 11a shows the rates of reduction of NO to N_2 , and Fig. 11b shows the overall rates of CH_4 oxidation to

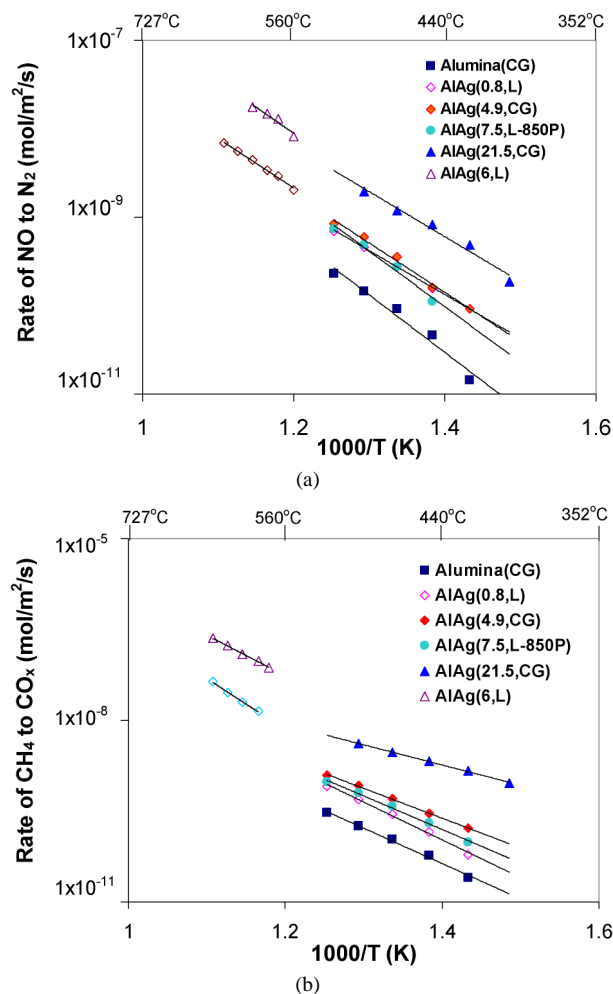


Fig. 11. Rates of $\text{CH}_4\text{-SCR}$ of NO_x over alumina and Ag–alumina (leached or as prepared); (a) rate of NO to N_2 ; (b) rate of the overall CH_4 oxidation reaction.

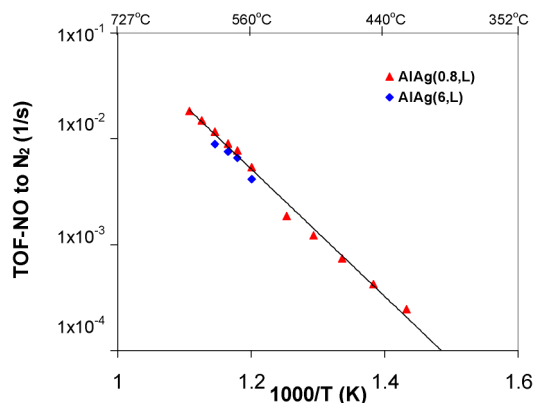


Fig. 12. TOF of NO to N₂ over leached Ag–alumina catalysts.

CO_x. Blank alumina exhibits the lowest rates of NO to N₂ and overall CH₄ oxidation. Doping with silver enhances the above rates, as shown for the rates over AlAg(0.8,L), AlAg(4.9,CG), and AlAg(7.5,L-850P). Interestingly, the rates for these samples are very close to one another. The similar rates of NO to N₂ in the leached sample, AlAg(0.8,L), and the parent sample, AlAg(4.9,CG), indicate that oxidized silver species are the sites responsible for the SCR, and that silver particles do not participate in CH₄-SCR of NO. AlAg(4.9,CG) displays higher overall rates of CH₄ oxidation than AlAg(0.8,L), which is consistent with the literature [42] that silver nanoparticles contribute to methane combustion and also with the CO₂ elution profiles during TPSR in Fig. 9c.

In Fig. 11a, for AlAg(0.8,L), the rates measured at C:N = 5 are comparable with the rates measured at the C:N = 1 condition after extension to lower temperatures. Hence, the C:N ratio does not affect the SCR reaction pathway.

For samples with higher silver amounts, such as AlAg(21.5, CG), significantly enhanced rates of NO to N₂ are observed. The rates over the corresponding leached sample AlAg(6,L) were similarly enhanced, and the activation energies were the same. For the leached AlAg(0.8,L) and AlAg(6,L), using the amount of silver present on the surface of these two catalysts to scale the rate, we can produce a TOF plot. The TOF values for NO to N₂ were calculated from the rates in Fig. 11a and the number of surface silver sites based on the XPS results (Table 1). As shown in Fig. 12, the TOF plots are in excellent agreement.

Table 4 gives the apparent activation energies, E_a , obtained from Fig. 11. For NO reduction to N₂, the E_a values for the Ag–alumina catalysts are in the range of 94.7–119.7 kJ/mol, whereas for Al₂O₃(CG), a slightly higher value of 123.8 kJ/mol is calculated. The E_a values for overall methane oxidation are in the range of 93.9–128 kJ/mol for alumina and low-silver content catalysts and 63.2 kJ/mol for AlAg(21.5,CG). Table 4 also lists the activation energies for CH₄-SCR of NO reported for other catalysts, including Co-ZSM-5, Sr/La₂O₃, and others. Interestingly, the E_a values for Ag–alumina catalysts reported here are very close to the activation energies reported for other very different CH₄-SCR catalysts. Whether this is indicative of a common methane activation step over all these catalysts remains unclear.

Table 4
Apparent activation energies of CH₄-SCR of NO_x over various catalysts

Sample	E_a -NO (kJ/mol)	E_a -CH ₄ (kJ/mol) ^a	Reductant	Reference
Al ₂ O ₃ (CG)	123.8	111.4	CH ₄	This work
AlAg(0.8,L)	94.7	118.8	CH ₄	This work
AlAg(4.9,CG)	106.4	93.9	CH ₄	This work
AlAg(6,L)	113.0	128.0	CH ₄	This work
AlAg(21.5,CG)	97.2	63.2	CH ₄	This work
AlAg(7.5,L-850P) ^b	119.7	105.5	CH ₄	This work
Ce–Ag–ZSM-5	98	87	CH ₄	[59]
Co–ZSM-5	91	102	CH ₄	[5]
La ₂ O ₃ , Sr/La ₂ O ₃	111.8	–	CH ₄	[60]
Sr/La ₂ O ₃ /Al ₂ O ₃	103.2	–	CH ₄	[61]
Li/MgO	147	–	CH ₄	[62]

^a Apparent activation energy of the overall methane oxidation reaction.

^b This sample is leached from an 850 °C-calcined parent; after leaching, it was calcined again at 650 °C for 3 h.

For HC-SCR of NO, the prevailing mechanisms found in the literature involve adsorbed nitrates and partially oxidized hydrocarbons [63], for which extensive in situ DRIFTS evidence exists. For Ag/alumina, nitrates and acetates are generally accepted as reaction intermediates in SCR of NO with reductants other than CH₄ [29,51,53,56]. However, the pathway for dinitrogen formation is still unclear, with species such as R–NO_x, isocyanate, cyanide, amines, and NH₃ proposed as possibilities [51]. For a reductant such as methane, an important mechanistic aspect is activation via abstraction of hydrogen from the C–H bond, which has been proposed to be the rate-determining step during CH₄-SCR of NO [64]. For Co-ZSM-5, adsorbed NO₂ on Co sites is reported to activate CH₄ [64], whereas a Pd ion can break the C–H bond directly, as has been proposed for Pd/H-ZSM-5 [65]. Direct activation of methane on Ag⁺ ions in Ag-ZSM-5 has been proposed by Shi et al. [47].

For the Ag–alumina system, our results show that the SCR-active NO_x species are adsorbed on alumina sites. How methane activation occurs is also indicated by the data of Figs. 9–12 taken collectively. First, methane is activated by adsorbed oxygen on silver nanoparticles at 300 °C, but this pathway leads to CO₂ only. No N₂ is produced from the nitrate species adsorbed on silver nanoparticles (see Figs. 8 and 9). The rate of N₂ production is the same for the parent and the leached catalysts, AlAg(4.9,CG) and AlAg(0.8,L), and AlAg(21.5,CG) and AlAg(6,L). But because the amount of strongly bound Ag⁺ is increased in the leached samples (e.g., from 0.8 to 6 wt%), the rate increases proportionately (see Fig. 12). We can surmise from this that the additional [Ag–O–Al] sites serve to activate more methane; thus, the reaction is limited by the activation of methane on Ag–alumina catalysts. Production of N₂ begins at ~300 °C from the interaction of adsorbed NO_x on alumina and CH_x species on Ag–O–Al groups (see Fig. 9). This scheme explains all of the data presented in this work. Fig. 13 shows a schematic of the mechanistic pathway. Although this pathway is plausible, future work should involve spectroscopic verification of the proposed reaction mechanism.

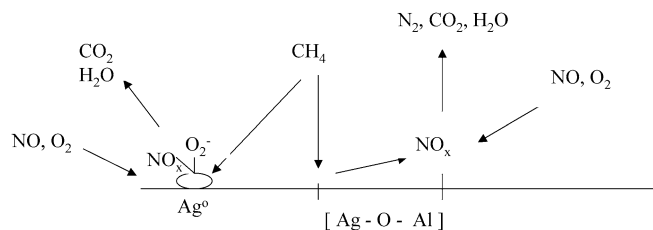


Fig. 13. Proposed reaction scheme for the selective catalytic reduction of NO with CH₄ over Ag–alumina.

4. Conclusion

In this work we investigated the role of silver nanoparticles, silver ions embedded in alumina, and alumina itself in the SCR of NO with methane under excess oxygen. Nitric acid leaching was used to remove silver particles and other weakly bound silver from Ag–alumina materials prepared by a coprecipitation-gelation method. For the leached catalysts, the surface silver content was found by XPS to be similar to the bulk value. UV–vis DRS identified silver cations and oxidized silver clusters and nanoparticles in the parent Ag–alumina catalysts. However, only ionic silver, bound with alumina, [Ag–O–Al], remained in the leached samples. The amount of ionic silver increases with increasing silver loading; that is, parent materials with high silver content have both more silver nanoparticles and more bound Ag–O–Al species. The SCR reaction rate scales with the number of [Ag–O–Al] sites.

NO–O₂–TPD tests revealed that the leached samples and bare alumina have the same NO_x adsorption features. Thus, bound silver ions cause no modification of the alumina surface sites. The presence of silver nanoparticles enhances the low-temperature NO_x adsorption peak. This species does not react with methane, which follows the direct oxidation route with adsorbed oxygen on the silver surface. N₂ production on alumina begins at 300 °C, as determined by TPSR. In contrast, transient reaction tests in CH₄–O₂ show that the light-off temperature for CH₄ combustion is above 470 °C for alumina, AlAg(0.8,L), and AlAg(6,L).

CH₄ combustion is much more facile on silver nanoparticles, with a light-off temperature of ~300 °C. This explains the lower selectivity of CH₄–SCR of NO over silver particle–laden Ag–alumina catalysts. Kinetic measurements demonstrated that the SCR reaction rates and activation energies are the same for the leached and parent Ag–alumina catalysts. The only advantage of the silver nanoparticles is the burnoff of CO produced over the Ag–O–Al structures.

On the basis of our findings, a plausible reaction pathway for SCR of NO with methane over Ag–alumina catalysts has emerged. Accordingly, CH_x species on [Ag–O–Al] react with NO_x adsorbed on alumina to produce dinitrogen.

Acknowledgments

Financial support of this work by a grant from the National Science Foundation (NIRT grant 0304515) is gratefully acknowledged. We thank Dr. Ed Neister for his assistance with the FTIR experiments.

References

- [1] H. Hamada, Y. Kintaichi, M. Sasaki, T. Ito, *Appl. Catal.* 64 (1990) L1.
- [2] Y. Li, J.N. Armor, *Appl. Catal. B* 1 (1992) L31.
- [3] Y. Li, J.N. Armor, *Appl. Catal. B* 2 (1993) 239.
- [4] Y. Li, J.N. Armor, *Appl. Catal. B* 3 (1993) L1.
- [5] Y. Li, P.J. Battavio, J.N. Armor, *J. Catal.* 142 (1993) 561.
- [6] Y. Li, J.N. Armor, *J. Catal.* 150 (1994) 376.
- [7] Y. Li, J.N. Armor, *Appl. Catal. B* 5 (1995) L257.
- [8] P. Budi, R.F. Howe, *Catal. Today* 38 (1997) 175.
- [9] E. Kikuchi, K. Yogo, *Catal. Today* 22 (1994) 73.
- [10] K. Yogo, M. Ihara, I. Terasaki, E. Kikuchi, *Chem. Lett.* (1993) 229.
- [11] K. Yogo, M. Ihara, I. Terasaki, E. Kikuchi, *Appl. Catal. B* 2 (1993) L1.
- [12] B.J. Adelman, W.M.H. Sachtler, *Appl. Catal. B* 14 (1997) 1.
- [13] R. Burch, J.P. Breen, F.C. Meunier, *Appl. Catal. B* 39 (2002) 283.
- [14] N. Li, A. Wang, L. Li, X. Wang, L. Ren, T. Zhang, *Appl. Catal. B* 50 (2004) 1.
- [15] K. Okumura, T. Kusakabe, M. Niwa, *Appl. Catal. B* 41 (2003) 137.
- [16] A. Bahamonde, S. Campuzano, M. Yates, P. Salerno, S. Mendioroz, *Appl. Catal. B* 44 (2003) 333.
- [17] N. Li, A. Wang, X. Wang, M. Zheng, R. Cheng, T. Zhang, *Appl. Catal. B* 48 (2003) 259.
- [18] N. Li, A. Wang, L.J. Tang, X. Wang, D. Liang, T. Zhang, *Appl. Catal. B* 43 (2003) 195.
- [19] M. Kantcheva, A.S. Vakkasoglu, *J. Catal.* 223 (2004) 364.
- [20] T. Miyadera, K. Yoshida, *Chem. Lett.* (1993) 1483.
- [21] N. Aoyama, K. Yoshida, A. Abe, T. Miyadera, *Catal. Lett.* 43 (1997) 249.
- [22] T.E. Hoost, R.J. Kudla, K.M. Collins, M.S. Chattha, *Appl. Catal. B* 13 (1997) 59.
- [23] K.A. Bethke, H.H. Kung, *J. Catal.* 172 (1997) 93.
- [24] T. Furusawa, K. Seshan, J.A. Lercher, L. Lefferts, K. Aika, *Appl. Catal. B* 37 (2002) 205.
- [25] M. Richter, M. Langpape, S. Kolf, G. Grubert, R. Eckelt, J. Radnik, M. Schneider, M.M. Pohl, R. Fricke, *Appl. Catal. B* 36 (2002) 261.
- [26] N. Bogdanchikova, F.C. Meunier, M. Avalos-Borja, J.P. Breen, A. Pestryakov, *Appl. Catal. B* 36 (2002) 287.
- [27] A. Martínez-Arias, M. Fernández-García, A. Iglesias-Juez, J.A. Anderson, J.C. Conesa, J. Soria, *Appl. Catal. B* 28 (2000) 29.
- [28] K. Shimizu, A. Satsuma, T. Hattori, *Appl. Catal. B* 25 (2000) 239.
- [29] K. Shimizu, J. Shibata, H. Yoshida, A. Satsuma, T. Hattori, *Appl. Catal. B* 30 (2001) 151.
- [30] L.-E. Lindfors, K. Eranen, F. Klingstedt, D.Yu. Murzin, *Top. Catal.* 28 (2004) 185.
- [31] F. Klingstedt, K. Eranen, L.-E. Lindfors, K. Eranen, S. Andersson, L. Cider, C. Landberg, E. Jobson, L. Eriksson, T. Ilkenhans, D. Webster, *Top. Catal.* 30/31 (2004) 27.
- [32] B. Wichterlova, *Top. Catal.* 28 (2004) 131.
- [33] K. Arve, L. Capek, F. Klingstedt, K. Eranen, L.-E. Lindfors, D.Yu. Murzin, J. Dedecek, Z. Sobalik, B. Wichterlova, *Top. Catal.* 30/31 (2004) 91.
- [34] T. Miyadera, *Appl. Catal. B* 13 (1997) 157.
- [35] T. Miyadera, *Appl. Catal. B* 16 (1998) 155.
- [36] T. Chafik, S. Kameoka, Y. Ukisu, T. Miyadera, *J. Mol. Catal. A* 136 (1998) 203.
- [37] S. Kameoka, T. Chafik, Y. Ukisu, T. Miyadera, *Catal. Lett.* 55 (1998) 211.
- [38] S. Kameoka, T. Chafik, Y. Ukisu, T. Miyadera, *Catal. Lett.* 51 (1998) 11.
- [39] S. Symiya, M. Saito, H. He, C. Qing, N. Takezawa, K. Yoshida, *Catal. Lett.* 50 (1998) 87.
- [40] A. Abe, N. Aoyama, S. Sumiya, N. Kakuta, K. Yoshida, *Catal. Lett.* (1998) 5.
- [41] A. Keshavaraja, X. She, M. Flytzani-Stephanopoulos, *Appl. Catal. B* 27 (2000) L1.
- [42] Lj. Kundakovic, M. Flytzani-Stephanopoulos, *Appl. Catal. A* 183 (1999) 35.
- [43] Z. Wang, M. Yamaguchi, I. Goto, M. Kumagai, *Phys. Chem. Chem. Phys.* 2 (13) (2000) 3007.
- [44] T. Nakatsuji, R. Yasukawa, K. Tabata, M. Niwa, *Appl. Catal. B* 17 (1998) 333.
- [45] K. Takagi, T. Kobayashi, H. Ohkita, T. Mizushima, N. Kakuta, A. Abe, K. Yoshida, *Catal. Today* 45 (1998) 123.

- [46] E. Seker, J. Cavataio, E. Gulari, P. Lorpongpaiboon, S. Osuwan, *Appl. Catal. A* 183 (1999) 121.
- [47] C. Shi, M. Cheng, Z. Qu, X. Bao, *Appl. Catal. B* 51 (2004) 171.
- [48] R. Burch, E. Halpin, J.A. Sullivan, *Appl. Catal. B* 17 (1998) 115.
- [49] A commercial software JADE was used for phase identification and lattice parameters calculation, which was coupled to ICDD Database.
- [50] G.B. Hoflund, Z.F. Hazos, *Phys. Rev. B* 62 (2000) 11126.
- [51] F.C. Meunier, J.P. Breen, V. Zuzaniuk, M. Olsson, J.R.H. Ross, *J. Catal.* 187 (1999) 493.
- [52] G.M. Underwood, T.M. Miller, V.H. Grassian, *J. Phys. Chem. A* 103 (1999) 6184.
- [53] K. Shimizu, H. Kawabata, A. Satsuma, T. Hattori, *J. Phys. Chem. B* 103 (1999) 5240.
- [54] S. Kameoka, Y. Ukisu, T. Miyadera, *Phys. Chem. Chem. Phys.* 2 (2000) 367.
- [55] F.C. Meunier, V. Zuzaniuk, J.P. Breen, M. Olsson, J.R.H. Ross, *Catal. Today* 59 (2000) 287.
- [56] K. Shimizu, J. Shibata, A. Satsuma, T. Hattori, *Phys. Chem. Chem. Phys.* 3 (2001) 880.
- [57] Mass spectrometer-library (MKS-PPT v4.24).
- [58] C. Shi, M. Cheng, Z. Qu, X. Yang, X. Bao, *Appl. Catal. B* 36 (2002) 173.
- [59] Z. Li, Ph.D. Thesis, Tufts University (1998).
- [60] X. Zhang, A.B. Walters, M.A. Vannice, *Appl. Catal. B* 7 (1996) 321.
- [61] C. Shi, A.B. Walters, M.A. Vannice, *Appl. Catal. B* 14 (1997) 175.
- [62] X. Zhang, A.B. Walters, M.A. Vannice, *J. Catal.* 146 (1994) 568.
- [63] O. Gorce, F. Baudin, C. Thomas, P. Da Costa, G. Djéga-Mariadassou, *Appl. Catal. B* 54 (2004) 69.
- [64] A.D. Cowan, R. Dumpelmann, N.W. Cant, *J. Catal.* 151 (1995) 356.
- [65] H. Kato, C. Yokoyama, M. Misono, *Catal. Today* 45 (1998) 93.